Computed tomography and magnetic resonance imaging features of cervical chordoma

JIU-FA CUI[1], DA-PENG HAO[1], HAI-SONG CHEN[1], JI-HUA LIU[1], FENG HOU[2] and WEN-JIAN XU[1]

Departments of [1]Radiology and [2]Pathology, Affiliated Hospital of Qingdao University, Qingdao, Shandong 266003, P.R. China

Received October 12, 2016; Accepted September 1, 2017

DOI: 10.3892/ol.2018.8721

Abstract. Computed tomography (CT) and magnetic resonance imaging (MRI) scans of 11 patients with histologically proven cervical chordoma were retrospectively evaluated. Imaging features assessed included location, morphology, association with adjacent structures, vertebral destruction, status of cortical bone, periosteal reaction, attenuation and calcification by CT, and signal intensity and enhancement pattern by MRI. Of 7 cases with CT, 6 exhibited lytic-sclerotic bone destruction. A total of 5 cases exhibited pressure erosion of outer cortex, 3 of which had spiculated periosteal reaction. Calcification was observed in 3 cases. All cases were heterogeneous and hypodense. MRI T2-weighted images (n=10) revealed heterogeneous hyperintense (n=5), intermediate (n=2) and intermediate-hyperintense signal intensity (n=3). Hypointense septa between lobules (n=5) and stripes (n=3) were observed on T2-weighted images. Post-contrast magnetic resonance images (n=6) demonstrated marked heterogeneous (n=3) and ring-like (n=3) enhancement. CT scanning is valuable in revealing the lytic-sclerotic bone destruction, pressure erosion of outer cortex and calcification. MRI is useful in demonstrating the results of soft tissue mass. The two examinations are necessary for differential diagnosis of patients with suspected cervical chordoma.

Introduction

Chordomas are rare malignant tumors exhibiting notochordal differentiation (1). The most common sites of tumor development include the sacrococcygeal region (50-60%), spheno-occipital region (25-35%) and mobile spine (15%) (2). Lesions of the cervical spine are rare, comprising between 3 and 7% of all chordomas, and between 20 and 50% of spinal chordomas (3). Lesions of the cervical spine are often overlooked as a diagnostic possibility in patients with neck pain or mass. The present study retrospectively reviewed the computed tomography (CT) and magnetic resonance imaging (MRI) results of 11 patients with chordoma of the cervical spine in an effort to evaluate the typical imaging features of these unusual lesions and to facilitate improved differential diagnosis from other lesions.

Correspondence to: Dr Wen-Jian Xu, Department of Radiology, Affiliated Hospital of Qingdao University, 16 Jiangsu Road, Qingdao, Shandong 266003, P.R. China
E-mail: cjr.xuwenjian@vip.163.com

Key words: computed tomography, magnetic resonance imaging, cervical spine, chordoma

Materials and methods

Patients. The present study was approved by the Institutional Review board of the Affiliated Hospital of Qingdao University. From between July 2008 and 2016, 11 cases of histologically proven cervical chordomas were selected and retrospectively reviewed. Pathological and clinical information including age at presentation and sex was also recorded.

Imaging techniques. CT scans were obtained using a standard CT protocol for the spine with multi-detector spiral CT scanner (LightSpeed; General Electric Healthcare Corporation, Waukesha, WI, USA). Scan type was helical (pitch/speed, 1.375:1, 13.75 mm). CT sections were imaged at 2.5 mm thickness with 2.5 mm space. MRI examinations were performed using a 3.0T magnetic resonance scanner (Signa HDx; GE Medical Systems Ltd., Little Chalfont, UK). Pre-contrast T1-weighted spin-echo images with and without fat saturation, and T2-weighted fast spin-echo images, and short T1 inversion recovery were obtained, followed by post-contrast T1-weighted spin-echo images with fat saturation following intravenous injection of 0.1 mmol/kg gadolinium dimeglumine. Images were obtained in at least two planes with 3 mm section thickness and 1 mm intersection gap.

Imaging analysis. CT and MRI studies were evaluated by two experienced radiologists using an image archiving and communication system, and results were determined by consensus. The following parameters were evaluated: Location of spine involvement, extension of soft tissue mass (anteriorly, laterally or posteriorly towards vertebrae), morphology (uni-lobular, multi-lobular or collar button), enlargement of transverse and intervertebral foramina, arterial encasement, disk involvement, bone destruction, status of cortical bone, periosteal reaction, attenuation and the presence of calcification by CT, signal intensity and enhancement pattern by MRI. Artery encasement was defined as circumferential contact

of tumor with vessel >270˚. The CT density was rated as hypodense, isodense or hyperdense compared with adjacent muscle. MRI signal intensity (SI) for the available sequences was compared with that of spinal cord and fat on T1-weighted images, with that of spinal cord and cerebrospinal fluid (CSF) on T2-weighted images. On T1-weighted images, it was classified as hypointense (SI<spinal cord), intermediate (spinal cord≤SI<fat) or hyperintense (SI=fat). On T2-weighted images, it was classified as hypointense (SI<spinal cord), intermediate (spinal cord≤SI<CSF), hyperintense (SI=CSF). The presence of hypointense septa was evaluated on T2-weighted images. On post-contrast MRI images, the degree of enhancement was subjectively assessed as mild enhancement (less than or equal to that of muscle) or marked enhancement (greater than that of muscle). The patterns of contrast enhancement were also recorded.

Results

There were 5 female and 6 male patients. The patients' ages ranged from between 15 and 75 years, with a mean age of 45.3 years and a median age of 48 years. Overall, the males (mean, 50.8 years; range, 18-64 years) were older than the females (mean, 44.5 years; range, 15-51 years). Tumors were identified from level of the C1 vertebra to C6. Vertebral body involvement was limited to a single level in 5 patients and were multi-level in 5 patients. Only 1 patient did not exhibit any vertebral body involvement, exhibiting only a uni-lobular intradural soft tissue mass (Fig. 1). Of the 10 patients with vertebral involvement, 9 exhibited soft tissue masses extended from adjacent vertebrae and 1 did not reveal any soft tissue mass. The soft tissue masses occurred anteriorly, laterally and posteriorly (n=5); anteriorly and laterally (n=3); and laterally and posteriorly (n=1) towards vertebrae in the axial plane (Fig. 2A). All 9 cases exhibited a multi-lobular soft tissue component which extended over the vertebrae involved and revealed a collar button appearance in the sagittal plane (Fig. 2B). Widening of the transverse foramen and intervertebral foramina was produced in 7 patients, and widening of only the transverse foramen in 2 patients. The vertebral artery was encased in 7 cases (Fig. 2A). Intervertebral disks were not affected in any of the cases.

Of the 7 cases with CT scans available, 6 revealed lytic-sclerotic bone destruction, 1 without distinct vertebral destruction. The feature of lytic-sclerotic bone destruction was similar to the melting ice or sequestrum within osteomyelitis (Fig. 2C). A total of 5 cases exhibited pressure erosion of the outer cortex (Fig. 2D), 3 of which had spiculated periosteal reaction (Fig. 2E). Pressure erosion is bone remodeling by a mass outside the bone. A total of 2 cases exhibited compression fractures. Calcification was demonstrated in 3/7 cases (Fig. 2C). All cases were heterogeneous and hypodense compared with adjacent muscle.

Of 10 cases with pre-contrast MRI images available, tumors were hypointense (n=6) or isointense (n=4) on T1-weighted images (Fig. 1A). Tumors were revealed to be hyperintense (n=5), intermediate (n=2) or intermediate-hyperintense (n=3) on T2-weighted images (Figs. 1B, 2A and B). Hypointense septa between lobules (n=5) and stripes in cases (n=3) were observed on the T2-weighted images (Fig. 2A). Of the 6 cases with post-contrast MRI images, 3 cases were heterogeneous and 3 cases exhibited ring-like enhancement (Fig. 1C).

The pathological results of all cases revealed a typical histological pattern of large cells with copious vacuolated cytoplasm separated by fibrous septa into lobules (Figs. 1D and 2F).

Discussion

Chordomas are considered to be aggressive, albeit slow growing, invasive and locally destructive (4). It has been hypothesized that chordomas arise from embryonic remnants of the primitive notochord (5). The tumor degenerates and disappears where it is surrounded by the vertebral bodies, but persists as the nucleus pulposus of each intervertebral disk. Remnants of the notochord may give rise to chordoma and usually remain in or close to the midline, entrapped within bone (5). However, there are a number of reports that chordoma may develop from a benign notochordal cell tumor (6-9). The tumor may occur at any age, but is usually observed in the fifth to seventh decades of life with male predilection (1).

Spinal chordomas typically develop within the vertebral body, primarily due to the association of the notochord with the developing axial skeleton (10). CT scanning may possess a potential advantage in detecting bone destruction, status of cortical bone, periosteal reaction and calcification. The majority of the present study demonstrated mixed lytic-sclerotic bone destruction which exhibited an appearance of melting ice or sequestrum within osteomyelitis (86%). Sclerosis may be due to reactive change of trabecular architecture (40-60%) (6,11,12). It has been identified that vertebral sclerosis may be a feature of chordoma (13). Lytic bone destruction with retention of trabecular architecture is a feature of aggressive yet slow growth, which is also frequently observed in vertebral hemangiomas (13). Furthermore, the extending soft tissue masses caused pressure erosion of the outer cortex and a spiculated periosteal reaction, as observed in the majority of the cases reviewed. The lesions typically produced widening of transverse and intervertebral foramina. These results also suggest aggressive but slow growth as a feature of the tumor. Calcification of the soft tissue mass occurred in 40% of cases as in the present series (14). The intratumoral calcifications were hypothesized to represent bone sequestrae from bone destruction or real calcifications of chondroid variant.

The presence of an accompanying soft tissue mass, spanning several vertebral levels, is characteristic of chordomas (15). Soft tissue mass without bone involvement, as observed in 1 of the cases reviewed, has been previously described (15-18). MRI is useful in demonstrating the soft tissue mass. Extension of the soft tissue mass was larger than the involved vertebral body which produces a collar button appearance in the sagittal plane. The lesions typically spare intervertebral disks, which may be involved in certain cases (2,19). Intervertebral disks were not affected in any of the cases reviewed. The soft tissue mass is usually multi-lobular and may occur anteriorly, laterally and posteriorly towards vertebrae in the axial plane. In the present study, the tumor occurred circumferentially (56%), anteriorly and laterally towards vertebrae (33%), and laterally and posteriorly towards vertebrae (11%). Encasement of the vertebral artery has been described previously (20). None of the tumors demonstrated vessel constriction (14). Signal

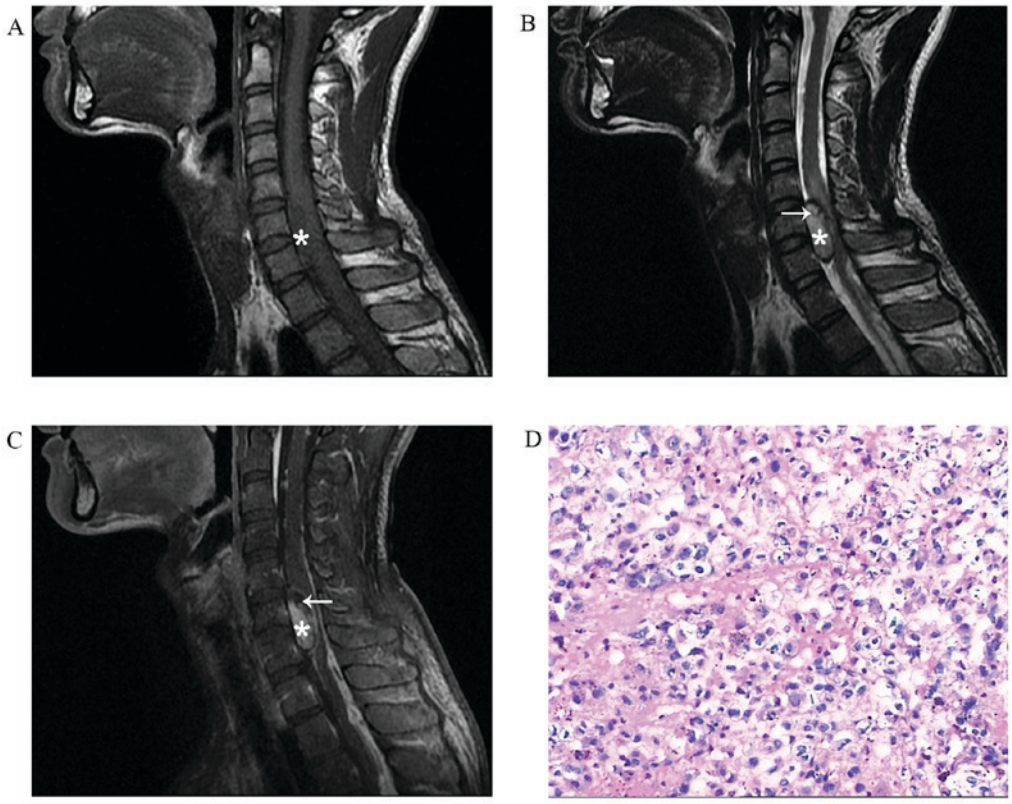

Figure 1. (A) Sagittal T1-weighted MRI revealed a lesion located in the spinal canal which is hypointense compared with spinal cord (asterisk). (B) Sagittal T2-weighted MRI revealed intermediate signal intensity (asterisk) with stripes (arrow). (C) Post-contrast sagittal fat-suppressed T1-weighted magnetic resonance image revealed heterogeneous and marked enhancement in the majority of regions of the lesion (asterisk) with an unenhanced hypointense region in the upper section (arrow). (D) Photomicrography revealed large cells with copious vacuolated cytoplasm separated by myxomatous stroma (hematoxylin and eosin; magnification, x100). MRI, magnetic resonance imaging.

intensity was heterogeneous and hyperintense with hypointense septa on T2-weighted images. The hyperintense signal intensity is the result of physaliphorous cells in myxomatous stroma of the chordoma. Hemorrhages, necrotic areas, calcification and sequestered bone fragments may explain the signal heterogeneity (15). The hypointense septa on T2-weighted images correspond to fibrous septa that divide the tumor. This feature is characteristic for diagnosing chordoma according to the literature and has been reported in 70% of tumors (21). Fibrous septa were identified in only 50% of the cases reviewed. However, stripes were identified in 30% of the patients. Enhancement patterns were heterogeneous or ringed. The cartilaginous components in the tumor may be responsible for the ringed enhancement pattern (15).

On the basis of the results of the present study and available literature, there are certain distinctive features of cervical chordoma including: Lytic and sclerotic bone destruction with soft tissue mass (collar button appearance in sagittal plane and multi-lobular surrounding the vertebrae in the axial plane); pressure erosion of outer cortex and spiculated periosteal reaction; widening of transverse and intervertebral foramina; encasement of the vertebral artery; calcification; heterogeneous and hypodense composition compared with the adjacent muscle on CT; heterogeneous and hyperintense composition equal to the CSF with hypointense septa on magnetic resonance T2-weighted images.

The aforementioned features above may be useful to distinguish chordoma from other lesions of the cervical spine. Benign notochordal cell tumor (BNCT) should be recognized for differential diagnosis of chordoma. Previous studies have documented the existence of BNCT within the axial skeleton (8,22). However, experience with these lesions is limited and distinction of BNCT from chordomas may not always be possible (23). Maintenance of trabecular architecture without bone destruction or expansion, lack of soft tissue extension and a lack of enhancement following contrast administration have been reported as the most reliable means of distinguishing between BNCT and chordoma radiographically (24,25). However, one study dispelled the hypothesis that any single radiological criterion used to distinguish between chordoma and BNCT is reliable (26). Hemangiomas may exhibit similar features; however, they may readily be distinguished by their CT appearances. Hemangiomas exhibit a polka dot appearance on axial images or a corduroy vertebra on sagittal images on CT scans. A number of cases without bone involvement have been described previously (15-18). In such cases, differentiation between chordoma and nerve sheath tumor may be difficult. However, a number of stripes may be identified in chordoma on magnetic resonance T2-weighted images (18). Furthermore, the location of the paravertebral tumor mass lateral and anterior to the vertebral body was not indicative of a tumor of nerve root origin (27). Tumor extension into the transverse foramina has not been reported in nerve sheath tumor (28). Chondrosarcoma exhibits similar MRI features with respect to chordoma, although it involves the neural arch

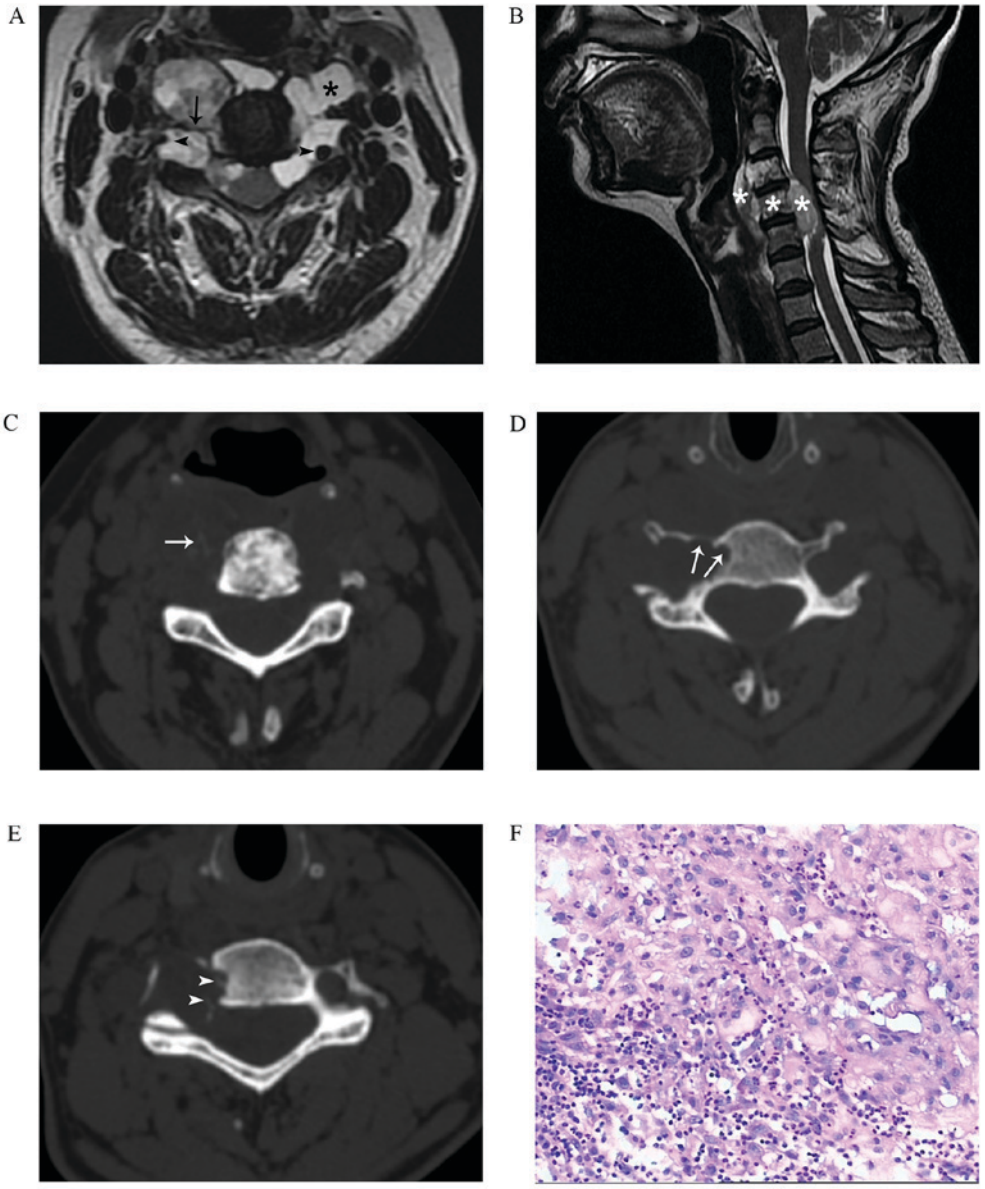

Figure 2. (A) Axial T2-weighted magnetic resonance imaging revealed that soft tissue mass locates anteriorly, laterally and posteriorly towards vertebrae and is hyperintense (asterisk) with hypointense septa between lobules (arrow). The two sides of vertebral arteries are encased (arrowhead). (B) Sagittal T2-weighted magnetic resonance image revealed so-called collar button appearance (asterisks) and tumor involvement of multi-level vertebrae. (C) Axial CT scan revealed lytic-sclerotic bone destruction which is similar to melting ice. Vague calcification may be observed right laterally (arrow). Axial CT scan revealed (D) pressure erosion of outer cortex (arrow) and (E) spiculated periosteal reaction (arrowheads). (F) Photomicrography revealed that the lesion consists of physaliphorous cells in myxomatous stroma and inflamed cells (hematoxylin and eosin; magnification, x100). CT, computed tomography.

more frequently than the vertebral body and the chondroid matrix is often evident as characteristic rings and arcs (27). Osteosarcoma may also demonstrate lytic-sclerotic destruction, but soft tissue mass of osteosarcoma often contains amorphous, cloud-like immature bone (11). Myeloma, lymphoma and spinal metastases may also be considered in the differential diagnosis. However, these tumors are often revealed to be more heterogeneous on T2-weighted images, and often occur in multifocal spinal localizations (11).

In conclusion, CT and MRI each have respective advantages in the diagnosis of chordoma. CT images have advantage of evaluating calcification and bone abnormalities that may narrow down the differential diagnosis to aggressive but slow-growing lesions, including mixed lytic-sclerotic bone destruction, pressure erosion of outer cortex and spiculated periosteal reaction. MRI scanning highlights features including multi-lobular hyperintensity on T2-weighted imaging with hypointense septa and soft tissue mass fully or partially surrounding vertebral body which may aid in the exclusion of the majority of lesions in the differential diagnosis. It is necessary to combine CT and MRI examinations for patients with suspected cervical chordoma.

Acknowledgements

Not applicable.

Funding

No funding was received.

Availability of data and materials

The datasets used and/or analyzed during the current study are available from the corresponding author upon reasonable request.

Authors' contributions

JFC was involved in designing of the study, analysis of data, drafting the manuscript and revising it. WJX and JHL made substantial contributions to conception, acquisition of data, and interpretation of data. DPH and HSC were responsible for the evaluation of CT and MRI images. FH was responsible for the associated pathological analysis. All authors have read and approved the final manuscript.

Ethics approval and consent to participate

The present study was approved by the Institutional Review board of the Affiliated Hospital of Qingdao University and informed consent was waived for this retrospective study.

Consent for publication

Not applicable.

Competing interests

The authors declare that they have no competing interests.

References

1. Christopher D, Fletcher JA and Krishnan U (eds): WHO classification of tumours of soft tissue and bone. International agency for research on cancer. 4th edition. WHO, Lyon, pp110-111, 2013.
2. Wippold FJ II, Koeller KK and Smirniotopoulos JG: Clinical and imaging features of cervical chordoma. AJR Am J Roentgenol 172: 1423-1426, 1999.
3. Bjornsson J, Wold LE, Ebersold MJ and Laws ER: Chordoma of the mobile spine. A clinicopathologic analysis of 40 patients. Cancer 71: 735-740, 1993.
4. Sundaresan N, Boriani S, Rothman A and Holtzman R: Tumors of the osseous spine. J Neurooncol 69: 273-290, 2004.
5. Erdem E, Angtuaco EC, Van Hemert R, Park JS and Al-Mefty O: Comprehensive review of intracranial chordoma. Radiographics 23: 995-1009, 2003.
6. Yamaguchi T, Yamato M and Saotome K: First histologically confirmed case of a classic chordoma arising in a precursor benign notochordal lesion: Differential diagnosis of benign and malignant notochordal lesions. Skeletal Radiol 31: 413-418, 2002.
7. Nishiguchi T, Mochizuki K, Tsujio T, Nishita T and Inoue Y: Lumbar vertebral chordoma arising from an intraosseous benign notochordal cell tumour: Radiological findings and histopathological description with a good clinical outcome. Br J Radiol 83: e49-e53, 2010.
8. Deshpande V, Nielsen GP, Rosenthal DI and Rosenberg AE: Intraosseous benign notochord cell tumors (BNCT): Further evidence supporting a relationship to chordoma. Am J Surg Pathol 31: 1573-1577, 2007.
9. Yamaguchi T, Watanabe-Ishiiwa H, Suzuki S, Igarashi Y and Ueda Y: Incipient chordoma: A report of two cases of early-stage chordoma arising from benign notochordal cell tumors. Mod Pathol 18: 1005-1010, 2005.
10. D'Haen B, De Jaegere T, Goffin J, Dom R, Demaerel P and Plets C: Chordoma of the lower cervical spine. Clin Neurol Neurosurg 97: 245-248, 1995.
11. Ross JS and Moore KR: Diagnostic imaging: spine. 3rd edition. Elsevier Health Sci, 2015.
12. Murphey MD, Andrews CL, Flemming DJ, Temple HT, Smith WS and Smirniotopoulos JG: From the archives of the AFIP. Primary tumors of the spine: Radiologic pathologic correlation. Radiographics 16: 1131-1158, 1996.
13. Darby AJ, Cassar-Pullicino VN, McCall IW and Jaffray DC: Vertebral intra-osseous chordoma or giant notochordal rest? Skeletal Radiol 28: 342-346, 1999.
14. Soo MY: Chordoma: Review of clinicoradiological features and factors affecting survival. Australas Radiol 45: 427-434, 2001.
15. Smolders D, Wang X, Drevelengas A, Vanhoenacker F and De Schepper AM: Value of MRI in the diagnosis of non-clival, non-sacral chordoma. Skeletal Radiol 32: 343-350, 2003.
16. Vaz RM, Pereira JC, Ramos U and Cruz CR: Intradural cervical chordoma without bone involvement. Case report. J Neurosurg 82: 650-653, 1995.
17. Dow GR, Robson DK, Jaspan T and Punt JA: Intradural cerebellar chordoma in a child: A case report and review of the literature. Childs Nerv Syst 19: 188-191, 2003.
18. Zhou H, Liu Z, Liu C, Ma Q, Liu X, Jiang L and Wei F: Cervical chordoma in childhood without typical vertebral bony destruction: Case report and review of the literature. Spine (Phila Pa 1976) 34: E493-E497, 2009.
19. Firooznia H, Pinto RS, Lin JP, Baruch HH and Zausner J: Chordoma: Radiologic evaluation of 20 cases. AJR Am J Roentgenol 127: 797-805, 1976.
20. Mortelé B, Lemmerling M, Mortelé K, Verstraete K, Defreyne L, Kunnen M and Vandekerckhove T: Cervical chordoma with vertebral artery encasement mimicking neurofibroma: MRI findings. Eur Radiol 10: 967-969, 2000.
21. Murphy JM, Wallis F, Toland J, Toner M and Wilson GF: CT and MRI appearances of a thoracic chordoma. Eur Radiol 8: 1677-1679, 1998.
22. Yamaguchi T, Suzuki S, Ishiiwa H, Shimizu K and Ueda Y: Benign notochordal cell tumors: A comparative histological study of benign notochordal cell tumors, classic chordomas, and notochordal vestiges of fetal intervertebral discs. Am J Surg Pathol 28: 756-761, 2004.
23. Yamaguchi T, Iwata J, Sugihara S, McCarthy EF Jr, Karita M, Murakami H, Kawahara N, Tsuchiya H and Tomita K: Distinguishing benign notochordal cell tumors from vertebral chordoma. Skeletal Radiol 37: 291-299, 2008.
24. Nishiguchi T, Mochizuki K, Ohsawa M, Inoue T, Kageyama K, Suzuki A, Takami T and Miki Y: Differentiating benign notochordal cell tumors from chordomas: Radiographic features on MRI, CT, and tomography. AJR Am J Roentgenol 196: 644-650, 2011.
25. Kyriakos M: Benign notochordal lesions of the axial skeleton: A review and current appraisal. Skeletal Radiol 40: 1141-1152, 2011.
26. Kreshak J, Larousserie F, Picci P, Boriani S, Mirra J, Merlino B, Brunocilla E and Vanel D: Difficulty distinguishing benign notochordal cell tumor from chordoma further suggests a link between them. Cancer Imaging 14: 4, 2014.
27. Elefante A, Caranci F, Del Basso De Caro ML, Peca C, Guadagno E, Severino R, Mariniello G and Maiuri F: Paravertebral high cervical chordoma. A case report. Neuroradiol J 26: 227-232, 2013.
28. Karakida O, Aoki J, Seo GS, Ishii K, Sone S, Nakakouji T and Otsuka K: Epidural dumbbell-shaped chordoma mimicking a neurinoma. Pediatr Radiol 26: 62-64, 1996.